Directed Self-Assembly of Nanoparticles for Nanomotors

Bin Dong,[†,‡] Tian Zhou,[‡] Hui Zhang,[†,‡] and Christopher Y. Li[‡,*]

[†]Institute of Functional Nano & Soft Materials (FUNSOM), Soochow University, Suzhou, Jiangsu 215123, China, and [‡]Department of Material Science and Engineering, Drexel University, Philadelphia, Pennsylvania 19104, United States

ABSTRACT We report, for the first time, the design and fabrication of a nanoparticle-based nanomotor system by directly self-assembling nanoparticles onto functional, nanometer-thin lamellae, such as polymer single crystals. Tens of thousands of judiciously selected nanoparticles (gold, iron oxide, and platinum nanoparticles) with sizes ranging from <5 to a few tens of nanometers have been introduced into a single nanomotor *via* directed self-assembly. The resulting nanomotor realizes functions such as autonomous movement, remote control, and cargo transportation by utilizing the advantages offered by nanoparticles, such as the small size, surface plasmon resonance, catalytic and magnetic properties. Because of the structural and functional versatility of nanoparticles, the facile fabricating procedure, and the potential for mass production, our strategy shows a key step toward the development of next generation multifunctional nanomotors.

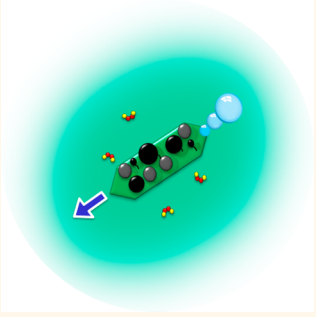

KEYWORDS: polymer single crystal · nanomotor · hybrid materials · nanoparticle · self-propelling

Inspired by biological motors,[1] man-made catalytic nanomotors, which are nanoscale devices that are capable of converting energy into forces and movement, have recently attracted increasing attention.[2−7] Since the discovery of the first man-made catalytic motor by Whitesides *et al.*,[2] the research field has experienced rapid progress.[3−17] Reported systems include bimetallic nanorods,[18] magnetically remote-controllable segmented nanorods,[19] and asymmetrically modified, microsphere-based, bubble-free motors.[20] Other developments include roll-up tube-based nanomotors fabricated by either a roll-up or template electrosynthesis method.[21−24] These tube-based nanomotors are capable of autonomous moving under physiological conditions[21] and nanobattery-based nanomotors.[22] In addition to providing autonomous motion, nanomotors have recently been used to sense ions[23] and to carry cargos[24] for cancer cell screening[25] or drug delivery.[26−28] By introducing functional materials during the motor fabrication process or performing post-surface modification, catalytic motors also can perform multifunctions. These fascinating artificial nanomachines hold unprecedented promises for applications in nanomachinery, nanomedicine, nanotransportation, and nanorobotics.

Many catalytic motors are based on asymmetric structures. In order to break mirror symmetry, reported synthesis strategies are mainly based on templating or microfabrication methods (lithography, metal deposition, *etc.*), which are not suitable for mass production purposes. The development of a symmetric motor that can be mass produced is therefore highly desirable. To date, only a few reports have studied symmetric motors. Kovtyukhova has carefully considered the orientation, movement, and gravitational forces of a particle in three-dimensional space and showed autonomous motion of a platinum rod motor in hydrogen peroxide solution.[29] Pantarotto *et al.* have also demonstrated similar motion of enzyme-decorated carbon nanotubes in glucose solution.[9] However, the above-mentioned methods suffer from either low-throughput or lack of control over the final structure. On the other hand, despite recent exciting progress in man-made motors, biological motors are far superior in terms of sophisticated functionality and small size, which are the two main challenges for current artificial motor systems.[8] To overcome these limitations, one promising candidate approach capable of achieving complex functionality at small scale is self-assembly, which allows for the construction of hierarchically complex nanostructures using basic building blocks.[30] To this end, Dreyfus *et al.* showed that a linear chain of colloidal

* Address correspondence to chrisli@drexel.edu.

Received for review February 22, 2013 and accepted May 6, 2013.

Published online May 06, 2013
10.1021/nn400925q

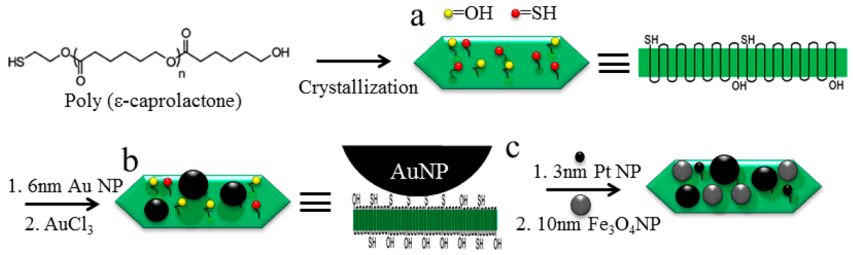

Scheme 1. Schematic illustrates the fabrication process of a nanoparticle-based nanomotor.

magnetic particles linked by DNA and attached to a red blood cell mimicked a flexible artificial flagellum; the entire ensemble can "swim" in a magnetic field.[13] Multicomponent nanomotors have also been fabricated by linking two (or several) particles *via* covalent or hydrophobic interaction.[10,24,31]

Herein, we report, for the first time, a nanoparticle-based nanomotor fabricated using a potentially scalable directed self-assembly method. Tens of thousands of judiciously selected nanoparticles with sizes ranging from <5 to a few tens of nanometers can be introduced into a single nanomotor *via* directed self-assembly, rendering unprecedented functional versatility. As a proof-of-concept, in this work, three different types of nanoparticles (*i.e.*, gold, iron oxide, and platinum nanoparticles; denoted as AuNP, Fe_3O_4NP, and PtNP, respectively) were directly self-assembled onto the surface of a quasi-two-dimensional polymer single crystal (PSC) to form a nanomotor. The functions of nanoparticles are as follows: AuNPs with tunable surface plasmon resonance (SPR) absorption serve as markers to make the nanomotor clearly visible under an optical microscope;[26,27] Fe_3O_4NPs allow for remote control with a magnetic field;[32] PtNPs are able to catalyze the decomposition of H_2O_2 to generate oxygen bubbles, providing the propulsion force. This nanoparticle-based multifunctional nanomotor is thin in one dimension (~90 nm) and can achieve all functions rendered by catalytic motors, including autonomous movement, remote control, and cargo transportation. Because nanoparticles are well-known for their high catalytic activity originated from the high surface area to volume ratio,[33] the introduction of catalytic active nanoparticles may lead to superior performances of the nanomotor. Other properties offered by nanoparticles can also be easily incorporated into the system. Our design thus opens up a great opportunity for the fabrication of nanoparticle-based nanomotors to meet the future requirement for diverse applications.

RESULTS AND DISCUSSION

PSC is the key to the present design because it provides the substrate for directed nanoparticle self-assembly. PSCs can be best formed *via* solution crystallization with a typical thickness of ~10 nm. Since their lateral sizes can reach hundreds of micrometers, PSCs are typically 2D in shape, mechanically flexible, and optically transparent. Recent work has demonstrated that, when end-functionalized polymer is used as the starting material, the resulting PSC can be used as a smart nanotape to immobilize nanoparticles, such as metallic nanoparticle,[34−36] Fe_3O_4NP,[37,38] or semiconducting quantum dots.[39] These results strongly suggest that, by judiciously selecting functional PSCs and nanoparticles, the latter can be assembled onto the PSC surface and the hybrid ensemble can serve as multifunctional nanomotors.

Scheme 1 illustrates the fabrication process to achieve this goal. PSC of α-hydroxyl-ω-thiol-terminated polycaprolactone (HO−PCL−SH)[40] was grown using a self-seeding method (Scheme 1a). PCL was used as the model polymer because controlled PSC can be readily formed using solution crystallization.[41] In particular, we chose α-hydroxyl-ω-thiol-terminated PCL since these two types of functional groups are chosen to enable conjugation of the PSC with targeted nanoparticles. During crystallization, because of the difference between polymer chain ends and the rest of the polymer backbone, the end-functional groups are excluded to the PSC surface,[42] making it rich of surface thiol and hydroxyl groups (smart "nanotape"). Figure 1a shows the low-magnification transmission electron microscopy (TEM) image of the PSC. The thickness of the PCL PSC is ~8 nm.[38] The areal number density of surface −SH or −OH functional groups is ~0.3/nm^2 on either surface of the single crystal, which can be calculated using the molecular weight of 9.2k g/mol, the two-chain orthorhombic unit cell of PCL with the unit cell parameter of a = 0.748 nm, b = 0.498 nm, and c = 1.726 nm,[43,44] and assuming all functional groups are excluded onto the surface of PSC.[45] Therefore, the overall number of surface −SH or −OH groups on the PCL single crystal is estimated to be around 3.2×10^7! This huge number of surface functional groups ensures our nanoparticle coupling. To this end, a AuNP was first immobilized onto the PSC surface through its interaction with thiol groups (Scheme 1b). Figure 1b shows a TEM image of the 6 nm AuNP-decorated PSC (PSC−$AuNP_6$ in abbreviation). Note that the AuNP does not immobilize onto PSC when surface −SH groups are absent, as demonstrated elsewhere.[34] PSC−$AuNP_6$ has an absorption peak around 529 nm originating from the SPR band of AuNP, as shown in Figure S1a in the Supporting Information. Note that pure PSC has no

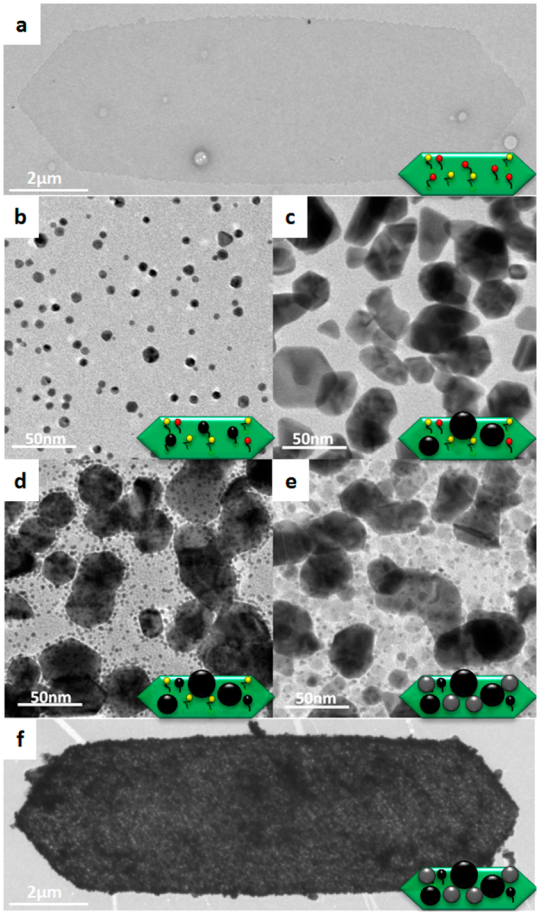

Figure 1. (a) Low-magnification TEM image of PSC. TEM images showing different fabrication stages of (b) PSC−Au_6, (c) PSC−Au_6 after $AuCl_3$ treatment, (d) PSC−AuNP−PtNP and (e) PSC−AuNP−PtNP−Fe_3O_4NP. (f) Low-magnification TEM image of PSC−AuNP−PtNP−Fe_3O_4NP.

absorption peak in the spectrum region from 400 to 1000 nm.[36] This structure showed weak contrast under an optical microscope due to the small size of the AuNP.

We then treated this PSC−Au_6 with $AuCl_3$ for 20 min, and the SPR band red-shifted to around 587 nm (Figure S1b in the Supporting Information), which indicates the formation of bigger AuNPs. Figure 1c shows the TEM image of the $AuCl_3$-treated PSC−Au_6 (denoted as PSC−AuNP). The PSC−AuNP structure is clearly visible under optical microscopy due to strong light absorption from the irregular AuNPs. They can then be considered as markers in the design. The surface coverage of AuNPs on PSC is approximately 55%, calculated using ImageJ. Considering that the surface −SH groups under AuNPs react with gold atoms to form S−Au bonds (Scheme 1b), the reacted −SH groups can then be estimated to be around 1.76×10^7, leaving the number of unreacted −SH groups to be about 1.44×10^7. We then treated this PSC−AuNP with 3 nm PtNP to synthesize PSC−AuNP−PtNP. Figure 1d shows that the PSC surface was able to adsorb a decent amount of PtNPs through Pt−thiol bonding. After this step, the surface coverage of AuNP and PtNP reaches 72%, indicating that the majority of surface −SH groups were consumed. Lastly, 10 nm Fe_3O_4NP was immobilized onto the PSC surface through the coupling between Fe_3O_4NP and the exposed hydroxyl groups (or remaining thiol groups), which were intact during the previous procedure due to the weak interaction between hydroxyl and AuNP/PtNP. Figure 1e,f shows the TEM image of the resulting PSC−AuNP−PtNP−Fe_3O_4NP. Because of the differences in size and contrast, three types of nanoparticles can be easily distinguished under TEM, such as big dark-colored irregular-shaped AuNPs, 10 nm sized light colored Fe_3O_4NPs, and 3 nm dark colored PtNPs. The total surface coverage of all three nanoparticles (AuNP, PtNP, and Fe_3O_4NP) on PSC reaches approximately 90%. Figure S2 in the Supporting Information shows a high-resolution TEM image indicating the lattice structures of three different types of nanoparticles (*i.e.*, 0.24 nm for AuNP(111), 0.23 nm for PtNP(111), and 0.26 nm for Fe_3O_4NP(311)). Figure S3 shows an AFM image of the as-fabricated PSC−AuNP−PtNP−Fe_3O_4NP, and the average thickness is measured to be approximately 90 nm. Therefore, the dimension of the PSC-based hybrid structure is $12\,\mu m \times 4\,\mu m \times 90$ nm (length/width/thickness). Note that the length and width of the PSC can be easily decreased to submicrometer range. The entire PSC−nanoparticle hybrid structure can also be viewed as a smart nanoshuttle, with PtNPs as the engine, Fe_3O_4NPs as the steering wheel, and AuNPs as the marker.

This nanoparticle-decorated PSC nanomotor (PSC−AuNP−PtNP−Fe_3O_4NP) moves autonomously when placed in a 15% H_2O_2 solution. Video S1 in the Supporting Information shows the large area view of the movement of this nanoparticle-based PSC motor. The average speed is estimated to be around 30 μm per second. Figure 2 and video S2 in the Supporting Information show an individual motor moving autonomously in circles. Since the PSC surface is homogeneously decorated with a dense layer of nanoparticles, the PSC-based nanomotor can then be considered as an analogue of the monocomponent catalytic nanorod in H_2O_2 solution, and the directional motion mechanism can be attributed to the momentum exchange between the nanomotor and water flux caused by oxygen bubble departure, driving the directional movement.[29] Detailed explanations for the self-propelling behavior of current micromotor are shown in Figure S4 in the Supporting Information. Until now, few researchers have focused on the relationship between motor speed and its composition. Here, we obtained the weight ratio between the catalytic part of the current motor (PtNP) and the noncatalytic part of the PSC-based nanomotor to be approximately 1:100 through TEM image analysis. This indicates that, due to the high catalytic activity, PtNP is capable of carrying the whole motor which is about 100 times its own body weight at a high speed (30 μm/s), demonstrating the

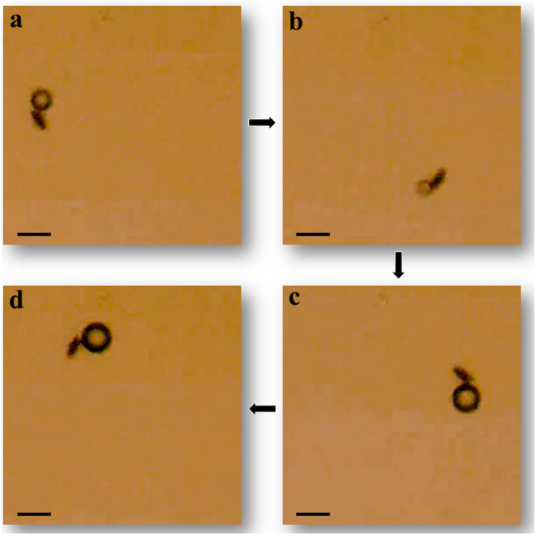

Figure 2. Series of optical images taken at 1 s interval showing the autonomous movement of the nanoparticle-based nanomotor. Scale bar: 20 μm. The corresponding movie is shown as video S2 in the Supporting Information.

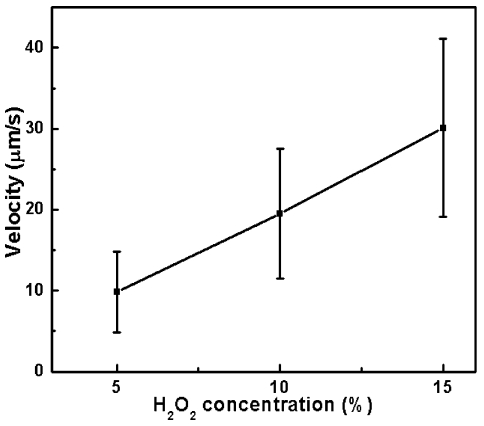

Figure 3. Velocity of the nanoparticle-based nanomotor at different hydrogen peroxide concentrations. Error bars indicate the standard deviation.

superiority of nanoparticle-based nanomotors. We have also tested the speed of the current motor in H_2O_2 with different concentrations. As shown in Figure 3, the average moving speed decreases from 30 μm/s in 15% H_2O_2 to about 20 and 10 μm/s in 10 and 5% H_2O_2, respectively. This result is consistent with the literature.[18]

Remote control of catalytic motors using an external field is of utmost importance since it allows for the control of moving directions to realize some of the essential functions of motors, such as cargo capture and delivery.[26] To this end, magnetic material has been introduced into motor systems by deposition methods; examples include nickel electrochemically deposited in the segmented nanorod[19] or thermally evaporated into roll-up tubes.[21] On the other hand, magnetic nanoparticles have unique superparamagnetic properties which has wide applications in information storage,[46] catalysis,[47] magnetic resonance imaging,[48] *etc.* The utilization of superparamagnetic material prevents the agglomeration caused by residual magnetism after removal of the magnetic field. In addition, the utilization of superparamagnetic material offers the possibility of being imaged by magnetic resonance imaging, which is beneficial for further *in vivo* biomedical applications related to nanomotors. To date, no superparamagnetic materials have been applied in nonbiological catalytic motor systems. Due to the small size, an individual Fe_3O_4NP has rather weak magnetic responses. In order to increase the magnetic responses of Fe_3O_4NPs, they have to be made in ensembles. As shown in Figure 1e, in our case, the surface of PSC can be covered with a dense layer of Fe_3O_4NPs. Therefore, our PSC template allows for the utilization of superparamagentic Fe_3O_4NPs as the magnetically responsive material in the fabrication of a nanomotor. Figure 4 shows a series of optical images indicating the trajectory of the nanoparticle-based nanomotor when applying a magnet at the up-left position. The nanoparticle-based nanomotor is quickly steered toward this direction. The corresponding movie is shown in the Supporting Information as video S3.

Cargo transportation represents one of the most promising applications related to nanomotors. A variety of cargoes, such as particles,[24] drugs,[26] and cells,[25] have been demonstrated. In order to test the capability of our current motor as the cargo carrier, we have utilized the magnetic polystyrene (PS) microparticle dispersed in water as the model cargo. As demonstrated by Wang *et al.*,[49] magnetic PS microparticles interact with the motor at its proximity to snap on for easy cargo capture. Figure 5a shows the nanoparticle-based nanomotor moving autonomously, propelled by the oxygen bubbles. Three different magnetic PS microspheres are shown, with the target PS microsphere labeled with a solid circle and two other PS microspheres labeled with dotted circles, which function as the marker to label the relative position from the target microsphere. As can be seen from video S4 in the Supporting Information, the nanoparticle-based motor was first slowed by applying an external magnetic field and then geared toward the target microsphere (indicated by the arrow in Figure 5). After capturing the cargo, the nanoparticle-based PSC carried it away, as indicated by the distance increase from the two PS microparticle markers (Figure 5b). Due to the strong magnetic interaction between the nanoparticle-based nanomotor and magnetic PS microspheres, it is difficult to release the current cargo. However, this problem could be solved by utilizing nonmagnetic material as the cargo. Furthermore, additional functional groups/receptors can be introduced onto the surface of the current nanomotor. A variety of specific cargos, including proteins, enzymes, and drugs, can then be loaded to realize some of the unique properties offered by nanomotors, such

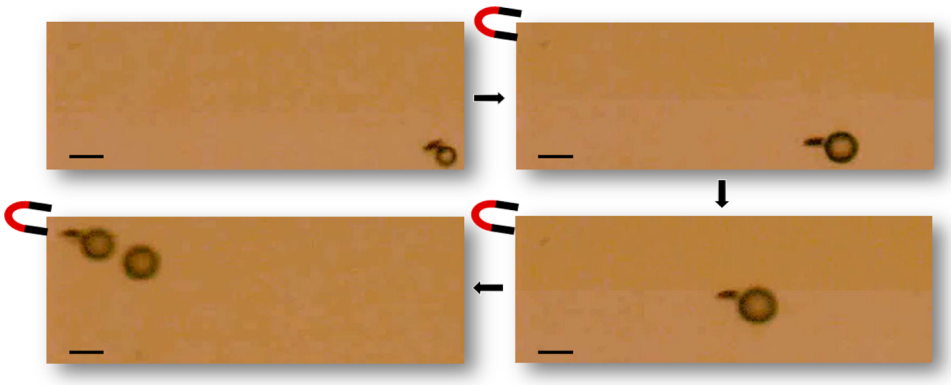

Figure 4. Series of optical images taken at 1 s interval showing the remote control of the nanoparticle-based PSC nanomotor under external magnetic field. The magnet is placed at the top left corner. Scale bar: 20 μm. The corresponding movie is shown as video S3 in the Supporting Information.

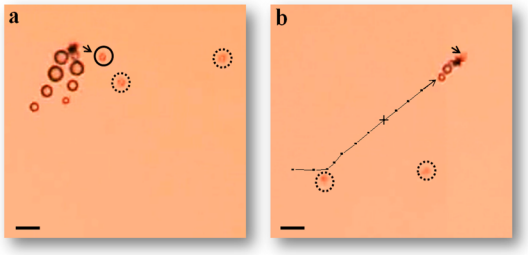

Figure 5. Cargo transportation using the nanoparticle-based nanomotor under an external magnetic field. These two images were captured at 8 s interval. The black curve in (b) indicates the trajectory of the nanomotor starting from (a), where the cross marks the position where the cargo is captured. Scale bar: 20 μm. The corresponding movie is shown as video S4 in the Supporting Information.

as targeted delivery, cell separations, *etc*. *In vivo* tests of such nanomotors will also be subjects of our future investigation.

CONCLUSION

In summary, we have shown using a directed nanoparticle self-assembly approach to fabricate an autonomously moving, magnetically steerable nanomotor system with all functions realized by nanoparticles with size ranging from <5 to a few tens of nanometers. This is achieved by coupling a variety of nanoparticles with distinct functions, including AuNPs, PtNPs, and Fe_3O_4NPs, onto the HO−PCL−SH PSC surface to form a tailored polymer/nanoparticle hybrid ensemble. Due to the SPR property of AuNPs, although thin in one dimension, the nanoparticle-based PSC nanomotor is clearly visible under an optical microscope. Because of the high catalytic activity, PtNP is capable of moving the whole nanomotor, which is around 100 times its own body weight, at a speed of 30 μm/s. Due to the Fe_3O_4NP ensemble on PSC, this nanomotor also allows for fast remote control and cargo transportation under a magnetic field. The size of PSC template can be easily controlled from a few tens of nanometers to hundreds of micrometers. The nanoparticle number density can also be controlled by varying the surface functional group areal density using end-functionalized polymers with different molecular weight.[34] We anticipate that a variety of end-functional polymers can be synthesized to form the smart PSC template to which various nanoparticles can attach. Since nanoparticles possess many unique properties, we believe this method has opened up a great opportunity for future miniaturization and mass production of nanomotors and for other applications including sensors and targeted deliveries.

EXPERIMENTAL SECTION

Materials. $AuCl_3$, ε-caprolactone, 2-mercaptoethanol, *Candida antarctica* lipase B (CALB), 1-butanol, iron oxide magnetic nanoparticles, and hydrogen peroxide were obtained from Sigma Aldrich Company. α-Hydroxyl-ω-thiol-terminated polycaprolactone (HO−PCL−SH, M_n = 9.2k) was synthesized using ring-opening polymerization of ε-caprolactone in the presence of 2-mercaptoethanol and CALB catalyst according to the literature.[40] Then, 6 nm AuNP and 3 nm PtNP were synthesized following literature methods.[50,51] Magnetic nanoparticle-coated polystyrene beads were purchased from Spherotech Inc.

Preparation of Nanoparticle-Based Nanomotor. Polymer single crystals were prepared using self-seeding method: 9 mg of HO-PCL-SH was dissolved in 30 g of 1-butanol at 60 °C for 10 min. Then the solution was brought to 5 °C for 2 h. The crystal solution was then heated at 46 °C for 10 min to obtain the crystal seeds. Finally, the solution was allowed to crystallize at 22 °C for 24 h. The suspension of the single crystals was isothermally filtered to remove uncrystallized polymers. To attach a 6 nm AuNP, polymer single crystal's 1-butanol solution was centrifuged and redispersed in pentyl acetate. AuNP solution was then added with 1:5 weight ratio and stirred for 24 h. Centrifugation was utilized to remove the free AuNP. This AuNP-decorated polymer single crystal was then treated using 10 mg/mL $AuCl_3$ pentyl acetate solution for 20 min, after which excess $AuCl_3$ was removed by centrifugation and redispersed in pentyl acetate. To attach the PtNP, a $AuCl_3$-treated polymer single crystal in pentyl acetate is mixed with PtNP solution with 1:1 weight ratio for 24 h. Centrifugation was utilized to remove free PtNP, and then the PtNP- and AuNP-decorated polymer single crystal was redispersed in pentyl acetate. Finally, Fe_3O_4NP solution was mixed with the above solution with 1:10 weight ratio for 24 h. Excess Fe_3O_4NP was

removed by centrifugation, and the final nanoparticle-decorated polymer single crystal was dispersed in water for the nanomotor study.

Characterization. UV−vis spectra were collected using an Ocean Optics USB4000 miniature fiber optic spectrometer at room temperature. TEM experiments were carried out using a JEOL JEM2100 TEM operated at an acceleration voltage of 200 kV. To prepare the TEM sample, one drop of single crystal suspension was cast on a carbon-coated nickel grid. After solvent evaporation, the sample was used for TEM observation without further treatment. AFM image was obtained on Digital Instrument Nanoscope IIIa. An Olympus BX51 microscope was employed to record the motion of the nanoparticle-based nanomotor, which was placed in hydrogen peroxide solution with different concentrations. To magnetically control the movement of the nanomotor, a neodymium (NdFeB) magnet was placed at a distance of 5 cm from the solution. The captured video was analyzed by PhysVis video motion analysis software.

Conflict of Interest: The authors declare no competing financial interest.

Acknowledgment. This work was supported by the NSF (DMR-0804838 and CMMI-1100166). TEM experiments were carried out at the Drexel's Centralized Research Facility.

Supporting Information Available: Figures S1−S4 and videos S1−S4. This material is available free of charge *via* the Internet at http://pubs.acs.org.

REFERENCES AND NOTES

1. Schnitzer, M. J.; Block, S. M. Kinesin Hydrolyses One ATP per 8-nm Step. *Nature* **1997**, *388*, 386–390.
2. Ismagilov, R. F.; Schwartz, A.; Bowden, N.; Whitesides, G. M. Autonomous Movement and Self-Assembly. *Angew. Chem., Int. Ed.* **2002**, *41*, 652–654.
3. Ozin, G. A.; Manners, I.; Fournier-Bidoz, S.; Arsenault, A. Dream Nanomachines. *Adv. Mater.* **2005**, *17*, 3011–3018.
4. Paxton, W. F.; Sen, A.; Mallouk, T. E. Motility of Catalytic Nanoparticles through Self-Generated Forces. *Chem.—Eur. J.* **2005**, *11*, 6462–6470.
5. Wang, J. Can Man-Made Nanomachines Compete with Nature Biomotors? *ACS Nano* **2009**, *3*, 4–9.
6. Ebbens, S. J.; Howse, J. R. In Pursuit of Propulsion at the Nanoscale. *Soft Matter* **2010**, *6*, 726–738.
7. Wang, J.; Manesh, K. M. Motion Control at the Nanoscale. *Small* **2010**, *6*, 338–345.
8. Mirkovic, T.; Zacharia, N.; Scholes, G. D.; Ozin, G. A. Nano-locomotion-Catalytic Nanomotors and Nanorotors. *Small* **2010**, *6*, 159–167.
9. Pantarotto, D.; Browne, W. R.; Feringa, B. L. Autonomous Propulsion of Carbon Nanotubes Powered by a Multienzyme Ensemble. *Chem. Commun.* **2008**, 1533–1535.
10. Vicario, J.; Eelkema, R.; Browne, W. R.; Meetsma, A.; La Crois, R. M.; Feringa, B. L. Catalytic Molecular Motors: Fuelling Autonomous Movement by a Surface Bound Synthetic Manganese Catalase. *Chem. Commun.* **2005**, 3936–3938.
11. Mano, N.; Heller, A. Bioelectrochemical Propulsion. *J. Am. Chem. Soc.* **2005**, *127*, 11574–11575.
12. Mirkovic, T.; Zacharia, N. S.; Scholes, G. D.; Ozin, G. A. Fuel for Thought: Chemically Powered Nanomotors Out-Swim Nature's Flagellated Bacteria. *ACS Nano* **2010**, *4*, 1782–1789.
13. Dreyfus, R.; Baudry, J.; Roper, M. L.; Fermigier, M.; Stone, H. A.; Bibette, J. Microscopic Artificial Swimmers. *Nature* **2005**, *437*, 862–865.
14. Ghosh, A.; Fischer, P. Controlled Propulsion of Artificial Magnetic Nanostructured Propellers. *Nano Lett.* **2009**, *9*, 2243–2245.
15. Hong, Y.; Blackman, N. M. K.; Kopp, N. D.; Sen, A.; Velegol, D. Chemotaxis of Nonbiological Colloidal Rods. *Phys. Rev. Lett.* **2007**, *99*, 178103.
16. Gibbs, J. G.; Kothari, S.; Saintillan, D.; Zhao, Y. P. Geometrically Designing the Kinematic Behavior of Catalytic Nanomotors. *Nano Lett.* **2011**, *11*, 2543–2550.
17. Gibbs, J. G.; Zhao, Y. Self-Organized Multiconstituent Catalytic Nanomotors. *Small* **2010**, *6*, 1656–1662.
18. Paxton, W. F.; Kistler, K. C.; Olmeda, C. C.; Sen, A.; St. Angelo, S. K.; Cao, Y. Y.; Mallouk, T. E.; Lammert, P. E.; Crespi, V. H. Catalytic Nanomotors: Autonomous Movement of Striped Nanorods. *J. Am. Chem. Soc.* **2004**, *126*, 13424–13431.
19. Kline, T. R.; Paxton, W. F.; Mallouk, T. E.; Sen, A. Catalytic Nanomotors: Remote-Controlled Autonomous Movement of Striped Metallic Nanorods. *Angew. Chem., Int. Ed.* **2005**, *44*, 744–746.
20. Pavlick, R. A.; Sengupta, S.; McFadden, T.; Zhang, H.; Sen, A. A Polymerization-Powered Motor. *Angew. Chem., Int. Ed.* **2011**, *50*, 9374–9377.
21. Solovev, A. A.; Mei, Y. F.; Urena, E. B.; Huang, G. S.; Schmidt, O. G. Catalytic Microtubular Jet Engines Self-Propelled by Accumulated Gas Bubbles. *Small* **2009**, *5*, 1688–1692.
22. Liu, R.; Sen, A. Autonomous Nanomotor Based on Copper-Platinum Segmented Nanobattery. *J. Am. Chem. Soc.* **2011**, *133*, 20064–20067.
23. Kagan, D.; Calvo-Marzal, P.; Balasubramanian, S.; Sattayasamitsathit, S.; Manesh, K. M.; Flechsig, G. U.; Wang, J. Chemical Sensing Based on Catalytic Nanomotors: Motion-Based Detection of Trace Silver. *J. Am. Chem. Soc.* **2009**, *131*, 12082–12083.
24. Sundararajan, S.; Lammert, P. E.; Zudans, A. W.; Crespi, V. H.; Sen, A. Catalytic Motors for Transport of Colloidal Cargo. *Nano Lett.* **2008**, *8*, 1271–1276.
25. Balasubramanian, S.; Kagan, D.; Hu, C. M. J.; Campuzano, S.; Lobo-Castanon, M. J.; Lim, N.; Kang, D. Y.; Zimmerman, M.; Zhang, L. F.; Wang, J. Micromachine-Enabled Capture and Isolation of Cancer Cells in Complex Media. *Angew. Chem., Int. Ed.* **2011**, *50*, 4161–4164.
26. Gao, W.; Kagan, D.; Pak, O. S.; Clawson, C.; Campuzano, S.; Chuluun-Erdene, E.; Shipton, E.; Fullerton, E. E.; Zhang, L. F.; Lauga, E.; *et al.* Cargo-Towing Fuel-Free Magnetic Nanoswimmers for Targeted Drug Delivery. *Small* **2012**, *8*, 460–467.
27. Wang, J.; Gao, W. Nano/Microscale Motors: Biomedical Opportunities and Challenges. *ACS Nano* **2012**, *6*, 5745–5751.
28. Wu, Y. J.; Wu, Z. G.; Lin, X. K.; He, Q.; Li, J. B. Autonomous Movement of Controllable Assembled Janus Capsule Motors. *ACS Nano* **2012**, *6*, 10910–10916.
29. Kovtyukhova, N. I. Toward Understanding of the Propulsion Mechanism of Rod-Shaped Nanoparticles That Catalyze Gas-Generating Reactions. *J. Phys. Chem. C* **2008**, *112*, 6049–6056.
30. Whitesides, G. M.; Boncheva, M. Beyond Molecules: Self-Assembly of Mesoscopic and Macroscopic Components. *Proc. Natl. Acad. Sci. U.S.A.* **2002**, *99*, 4769–4774.
31. Gao, W.; Pei, A.; Feng, X. M.; Hennessy, C.; Wang, J. Organized Self-Assembly of Janus Micromotors with Hydrophobic Hemispheres. *J. Am. Chem. Soc.* **2013**, *135*, 998–1001.
32. Gao, J. H.; Gu, H. W.; Xu, B. Multifunctional Magnetic Nanoparticles: Design, Synthesis, and Biomedical Applications. *Acc. Chem. Res.* **2009**, *42*, 1097–1107.
33. El-Sayed, M. A. Some Interesting Properties of Metals Confined in Time and Nanometer Space of Different Shapes. *Acc. Chem. Res.* **2001**, *34*, 257–264.
34. Li, B.; Li, C. Y. Immobilizing Au Nanoparticles with Polymer Single Crystals, Patterning and Asymmetric Functionalization. *J. Am. Chem. Soc.* **2007**, *129*, 12–13.
35. Wang, B. B.; Li, B.; Zhao, B.; Li, C. Y. Amphiphilic Janus Gold Nanoparticles *via* Combining "Solid-State Grafting-to" and "Grafting-from" Methods. *J. Am. Chem. Soc.* **2008**, *130*, 11594–11595.
36. Dong, B.; Wang, W. D.; Miller, D. L.; Li, C. Y. Polymer-Single-Crystal@Nanoparticle Nanosandwich for Surface Enhanced Raman Spectroscopy. *J. Mater. Chem.* **2012**, *22*, 15526–15529.
37. Dong, B.; Li, B.; Li, C. Y. Janus Nanoparticle Dimers and Chains *via* Polymer Single Crystals. *J. Mater. Chem.* **2011**, *21*, 13155–13158.
38. Dong, B.; Miller, D. L.; Li, C. Y. Polymer Single Crystal As Magnetically Recoverable Support for Nanocatalysts. *J. Phys. Chem. Lett.* **2012**, *3*, 1346–1350.

39. Wang, B. B.; Li, B.; Ferrier, R. C. M.; Li, C. Y. Polymer Single Crystal Templated Janus Nanoparticles. *Macromol. Rapid Commun.* **2010**, *31*, 169–175.
40. Hedfors, C.; Ostmark, E.; Malmstrom, E.; Hult, K.; Martinelle, M. Thiol End-Functionalization of Poly(ε-caprolactone), Catalyzed by *Candida antarctica* Lipase B. *Macromolecules* **2005**, *38*, 647–649.
41. Geil, P. H. *Polymer Single Crystal*; Interscience: New York, 1963.
42. Li, C. Y. Polymer Single Crystal Meets Nanoparticles. *J. Polym. Sci., Part B: Polym. Phys.* **2009**, *47*, 2436–2440.
43. Chatani, Y.; Okita, Y.; Tadokoro, H.; Yamashita, Y. Structural Studies of Polyesters. III. Crystal Structure of Poly-ε-caprolactone. *Polym. J.* **1970**, *1*, 555–562.
44. Hu, H.; Dorset, D. L. Crystal Structure of oly(ε-caprolactone-). *Macromolecules* **1990**, *23*, 4604–4607.
45. Zhou, T.; Wang, B.; Dong, B.; Li, C. Y. Thermoresponsive Amphiphilic Janus Silica Nanoparticles *via* Combining "Polymer Single-Crystal Templating" and "Grafting-from" Methods. *Macromolecules* **2012**, *45*, 8780–8789.
46. Sun, S. H. Recent Advances in Chemical Synthesis, Self-Assembly, and Applications of FePt Nanoparticles. *Adv. Mater.* **2006**, *18*, 393–403.
47. Schatz, A.; Reiser, O.; Stark, W. J. Nanoparticles as Semiheterogeneous Catalyst Supports. *Chem.—Eur. J.* **2010**, *16*, 8950–8967.
48. Meng, X. T.; Seton, H. C.; Lu, L. T.; Prior, I. A.; Thanh, N. T. K.; Song, B. Magnetic CoPt Nanoparticles as MRI Contrast Agent for Transplanted Neural Stem Cells Detection. *Nanoscale* **2011**, *3*, 977–984.
49. Burdick, J.; Laocharoensuk, R.; Wheat, P. M.; Posner, J. D.; Wang, J. Synthetic Nanomotors in Microchannel Networks: Directional Microchip Motion and Controlled Manipulation of Cargo. *J. Am. Chem. Soc.* **2008**, *130*, 8164–9165.
50. Toshima, N.; Yamada, Y.; Hirai, H. Colloidal Platinum Catalyst for Light-Induced Hydrogen Evolution from Water. A Particle Size Effect. *Chem. Lett.* **1981**, 793–796.
51. Jana, N. R.; Peng, X. G. Single-Phase and Gram-Scale Routes toward Nearly Monodisperse Au and Other Noble Metal Nanocrystals. *J. Am. Chem. Soc.* **2003**, *125*, 14280–14281.